ChemComm

COMMUNICATION

High-resolution mapping and recognition of lipid domains using AFM with toxin-derivatized probes

Received 00th January 20xx,
Accepted 00th January 20xx

DOI: 10.1039/x0xx00000x

www.rsc.org/

Andra C. Dumitru,*[a] Louise Conrard,*[b] Cristina Lo Giudice,[a] Patrick Henriet,[b] Maria Veiga-da-Cunha,[b] Sylvie Derclaye,[a] Donatienne Tyteca,[b] and David Alsteens[a†]

Cellular membrane lateral organization and in particular the assembly of lipids in domains is difficult to evaluate at high-resolution. Here, we used atomic force microscopy (AFM) to investigate at high-resolution lipid membranes containing variable amouts of sphingomyelin (SM) and cholesterol (Chol), two abundant membrane lipids. To this end, we developed new AFM tip functionalization strategies to specifically probe SM and Chol. Multiparametric AFM imaging allowed us to highlight the lateral submicrometric organization of these two lipids within lipid bilayers through the simultaneous topographic evidence of different phase regimes together with the extraction of their nanomechanical properties and the specific detection of lipid moieties by functionalized AFM probes. The combination of AFM topography and nanomechanical mapping with specific probes for molecular recognition of lipids represents a novel approach to identify lipid-enriched domains in supported bilayers and offers a unique perspective to directly observe lipid assemblies on living cells.

In recent years, increasing evidence linked lipid submicrometric domains and rafts to several key biological functions, such as protein and lipid sorting, cell-cell signalling, immune response, viral pathogenesis or endo- and exocytosis[1, 2]. Currently, most evidence of lipid domains relies on the use of fluorescence microscopy or spectroscopy techniques[3]. Nevertheless, direct observation of the architecture and structure-function relationship of these assemblies remains challenging due to their small size, dynamics and the lack of adequate imaging techniques with sufficient spatial and/or temporal resolution. Most of the methodologies currently used exploit fluorescent lipid analogs or stains, which have recently been object of increasing concerns regarding their suitability to evidence lipid submicrometric assemblies. Studies suggested that the covalent attachment of even a small fluorophore to a lipid molecule could abolish its ability to associate with rafts[4]. More recently, innovative approaches relied on the use of fluorescent proteins with phospholipid binding domain antibodies, Fab fragments or toxin fragments[5-9]. The prototype of these toxins is Cholera Toxin, a multi-complex protein that binds to GM1 ganglioside. One of the best-characterized cholesterol(Chol)-dependent cytolysins is Theta toxin that consists of four domains, The D4 domain being the minimal toxin fragment able to bind Chol with high affinity without causing lysis[10]. Membrane Chol-enriched domains has been demonstrated in living red blood cells using a truncated Theta limited to its C-terminal D4 domain (Theta-D4) fused with mCherry[11]. Similarly, non-Toxic Lysenin (NT-Lysenin), a fragment of Lysenin, the pore-forming toxin able to bind to sphingomyelin (SM) has been developed to target SM lipids while preventing oligomerization and/or pore formation[12, 13]. Upon fusion with mCherry, Lysenin allowed to reveal SM-enriched domains at the red blood cell surface[14]. Thus, among toxin probes, Theta toxin or Lysenin derivatives appeared as the most promising thanks to their monomeric state[15, 16]. Nevertheless, their size could affect lipid properties such as lateral diffusion after membrane labelling, underlying the importance of investigating membrane organization in their native state, *i.e.* without labelling with lipid probes.

In this context, AFM appears as a unique method that can simultaneously image at high-resolution biological samples in native conditions, while mapping mechanical and physico-chemical properties[17]. Thanks to its excellent signal-to-noise ratio, subnanometric resolution in height can be achieved allowing height differences to be observed between lipids existing in different phase regimes[18]. Recently, force-distance curve-based AFM (FD curve-based AFM) imaging was further developed enabling higher data acquisition speeds while maintaining sufficient precision (0.5 nm) for high-resolution imaging[19]. Importantly, the force sensitivity achieved (≈ 10 pN)

[a] *Louvain Institute of Biomolecular Science and Technology, Université catholique de Louvain, Croix du sud 4-5, 1348 Louvain-La-Neuve, Belgium.*
[b] *de Duve Institute, Université catholique de Louvain, Avenue Hippocrate 75, 1200 Woluwe-Saint-Lambert, Belgium.*
* A.C.D. and L.C. contributed equally.
† Correspondence: david.alsteens@uclouvain.be
Electronic Supplementary Information (ESI) available: [details of any supplementary information available should be included here]. See DOI: 10.1039/x0xx00000x

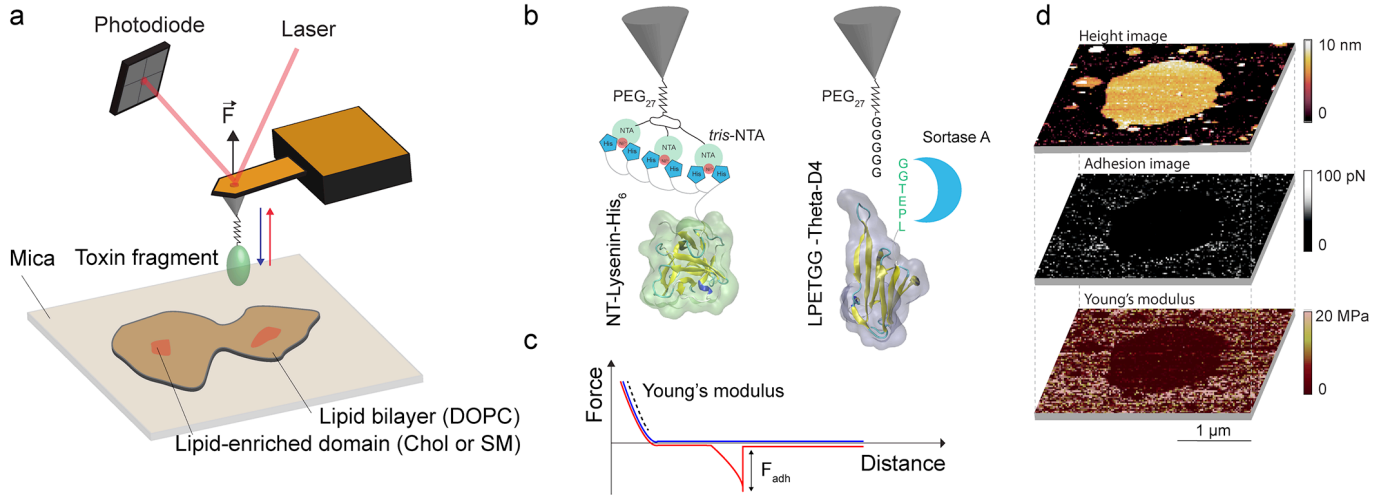

Fig. 1 High-resolution FD curve-based AFM imaging of supported bilayer with toxin derivatized AFM tips. (a) Schematics of the force spectroscopy experiments performed between a toxin fragment grafted on the AFM tip and a supported bilayer (DOPC/Chol or DOPC/SM). The AFM tip is approached (blue arrow) and retracted (red arrow) from the surface and the force is monitored using a laser focused on the AFM cantilever and deflected into a photodiode resulting in a force vs distance curve. (b) The AFM tip is functionalized with a PEG spacer fused to either a tris-nitrilotriacetate-Ni^{2+}(*tris*-NTA) or a hexaglycine peptide, which in turn react respectively with the His6-tagged Lysenin toxin or with the LPETGG-Theta-D4 via the sortase A enzyme. (c) The recorded tip-sample interactions are displayed as force-distance (FD) curves. Mechanical properties (including adhesion) can be extracted from individual force curves and directly correlated with the position on the sample allowing the reconstruction of maps (d).

biological samples in their physiological state. Combined with functionalized probes, this tool can be extended to a powerful sensor allowing the localization of individual molecules or molecular assemblies at the nanoscale with high specificity[4, 20, 21]. To date, however, such high-resolution imaging of native membranes together with the identification of specific lipids has not been demonstrated.

Here, we report the use of FD curve-based AFM with tips functionalized with toxin fragments (Theta-D4 (θ) and Lysenin derivatives) to image and identify Chol- and SM-enriched lipid domains within 1,2-dioleoyl-*sn*-glycero-3-phosphocholine (DOPC) at high-resolution (Fig. 1a). Our findings demonstrate that AFM force spectroscopy with specific probes is a direct and simple approach for identifying the preferential localization of specific lipids without any fixation or labelling steps. In addition, high-resolution height images and Young's modulus variation provide additional evidence of lateral heterogeneities in lipid membranes.

To maximize binding efficiency, we opted for a tip chemistry that ensures the oriented grafting of the toxin fragments on the AFM tip. To this end, both toxins were labelled with specific tags (Fig. 1b and Fig S1). Lysenin was labelled with a hexa-histidine tag (His_6 tag) and tethered to a *tris*-NTA functionalized tip (see supplementary material for details). θ toxin was flanked by a LPETGG sequence and bound to the hexaglycine tip using a sortase-mediated reaction (see supplementary material for details, page S1)[22].

Using FD curve-based AFM we imaged model lipid bilayers adsorbed onto freshly cleaved mica in Tris-buffer solution. For every pixel of the AFM topography image a FD curve was recorded (Fig. 1c). The maximum force applied was set up to 100 pN (see supplementary material for other details, page S2). From every FD curve recorded, the Young's modulus of elasticity and the adhesion were extracted from a fit with the Hertz model in the repulsive part of the approach curve[23] and from the retraction curve respectively (Fig. 1c), and displayed as maps using coloured vertical scales (Fig. 1d).

We first imaged DOPC:SM (70:30) supported bilayers on mica with a Lysenin-derivatized AFM tip (Fig. 2). The height image revealed nanometric and submicrometric lateral heterogeneities. Adhesion and Young's modulus channels clearly show that these areas correspond to stiffer and more adhesive regions suggesting that these domains are enriched in SM. Notably, the adhesion channel reveals clear differences between lipid phase underlying that Lysenin appears as an ideal tool to put in evidence SM-enriched lipid phases. In addition, the adhesion force remains stable over the whole image and individual FD curves present single rupture events with force ranging from 150 ± 50 pN, in good agreement with single-molecule rupture forces. Finally, simultaneous cross-sections performed on the various AFM channels highlight the convergence of this multiparametric approach. At high-resolution, as can be achieved on supported bilayers, topographical heterogeneities perfectly coincided with local variations in both the adhesion and Young's modulus channels. This also indicates that the lateral resolution obtained in the adhesion channel is not strongly affected by the linker length used to graft the toxin to the tip. Control experiments performed with a Lysenin-tip on lipid bilayers lacking the SM component showed no specific adhesion events (Fig. S2a-c). Also, when the DOPC:SM bilayer was probed with a bare AFM tip, the adhesion channel showed no contrast, while the Young's modulus maps did display local heterogeneities in nanomechanical properties (Fig. S3). This result indicates that the toxin fragment present on the AFM tip does not induce SM domains.

Similarly, we also performed experiments on DOPC:Chol (70:30) supported bilayers on mica with the θ toxin fragment

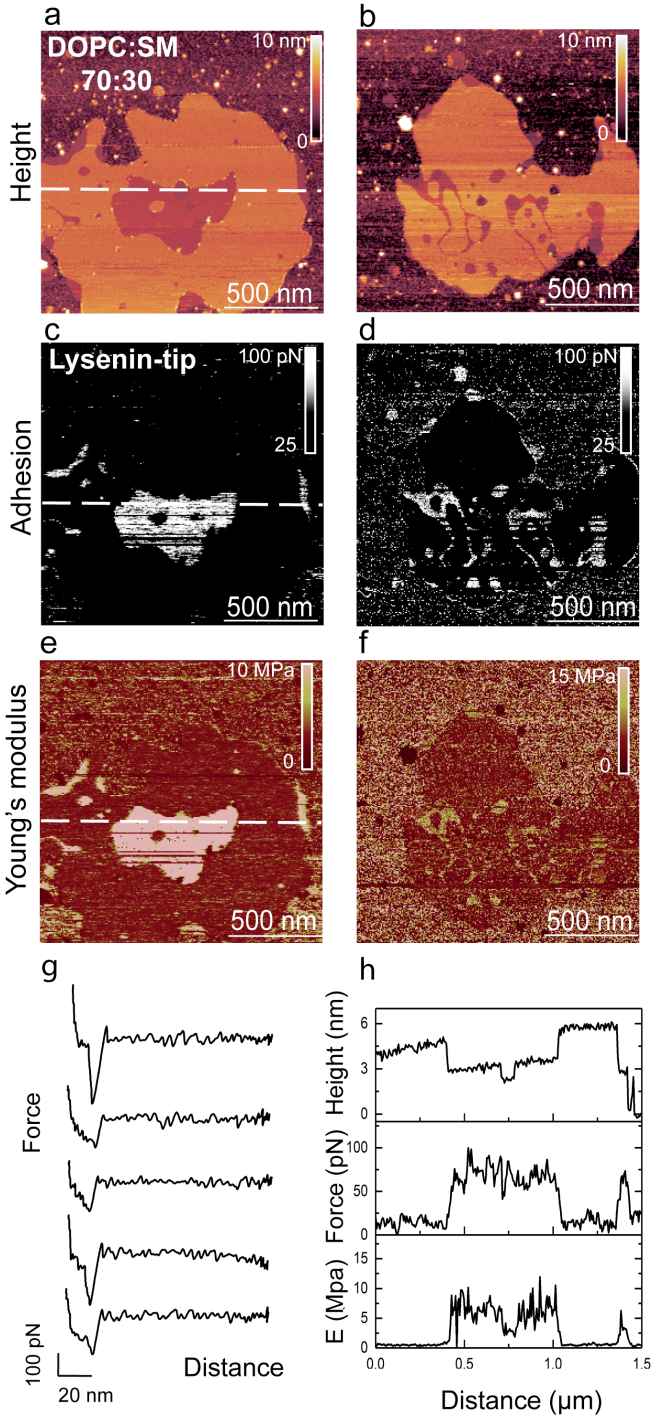

Fig 2. Mapping SM-enriched domains with a Lysenin AFM tip on DOPC:SM (70:30) lipid bilayers. (a,b) FD-based AFM height images and corresponding (c,d) adhesion and (e,f) Young's modulus maps. (g) Representative force-distance curves recording specific unbinding events between the Lysenin tip and SM-enriched domains. Adhesion peaks appear 10-20 nm away from the surface and rupture forces are in the range of 100-200 pN. (h) Simultaneous height, adhesion force and Young's modulus (E) cross-section profiles extracted from the corresponding maps in (a,c,e). SM-enriched domains show specific topographical features that are correlated with local maxima in force and E values.

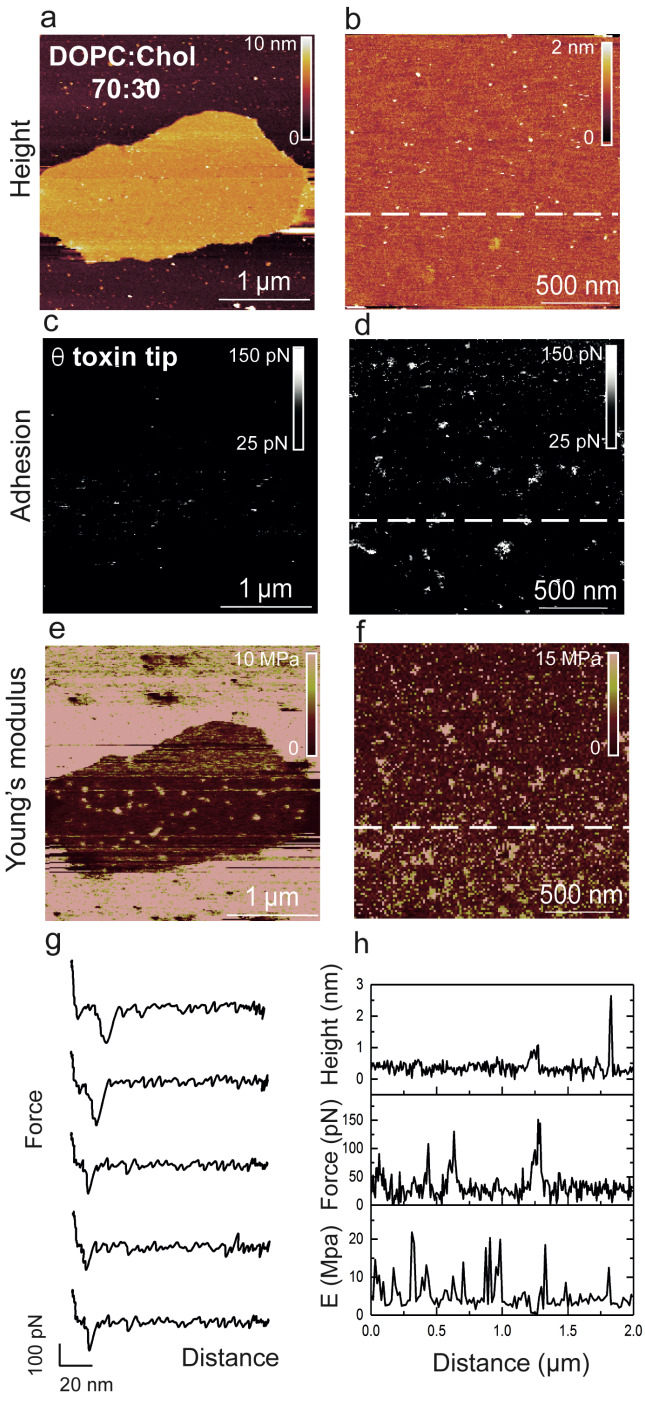

Fig 3. Mapping Chol-enriched domains with a θ-functionalized AFM tip on DOPC:Chol (70:30) lipid bilayers. (a) Overview topography (height) images of a lipid patches on mica and (b) high-resolution height image of the bilayer. Corresponding (c,d) adhesion and (e,f) Young's modulus maps. (g) Representative force-distance curves recording specific unbinding events between the θ tip and Chol-enriched domains. Adhesion peaks appear 10-20 nm away from the surface and rupture forces are in the range of 100-150 pN. (h) Simultaneous height, adhesion force and Young's modulus (*E*) cross-section profiles extracted from the corresponding maps in (b,d,f). Chol-enriched domains with or without topographical features are correlated with maxima in force and *E* values.

grafted onto the AFM tip. Overview images of the bilayers showed a mica surface covered with lipid patches (Fig 3a). High-resolution images (Fig. 3b, S4a-c and S5) only show very small lateral heterogeneities (~20-40 nm in diameter Fig. S4d-g). The adhesion channel revealed that the θ toxin tip shows only sparsely distributed adhesion events along with some clusters. Molecular recognition events between the θ toxin tethered on the AFM tip and Chol-enriched domains were in

the range of 100 ± 50 pN. The adhesion events co-localize with stiffer areas, as shown in the cross-sections in Fig. S4d-g, which is in good agreement with the coexistence of a lipid DOPC:Chol phase, surrounded by a lipid disordered phase[24, 25]. The height, adhesion and Young's modulus channels in Fig. 3 reveal the existence of two types of Chol-enriched domains, both of nanometric size: (*i*) adhesive and stiffer domains with no topographical features and (*ii*) adhesive and stiffer domains that protrude 0.3-1 nm from the lipid bilayer. As predicted by Ursell *et al.,* in the context of lipid rafts, lipid domains can adopt a flat or dimpled morphology. In the latter case, this dimpled morphology facilitates a repulsive interaction that slows coalescence and helps regulate domain size[26]. This transition between dimpled and flat morphology depends on various factors such as the bilayer elastic properties and the domain size. Our data suggest that the dimpled domains are the larger ones with an average diameter of 20 ± 10 nm for flat domains (N=40) and 40 ± 20 nm for dimpled domains (N=25), as determined from the adhesion and Young's modulus channels. To confirm the specificity of the observed interactions between the θ toxin AFM tip and the DOPC:Chol lipid bilayer, we performed two different control experiments. First, a bare AFM tip showed no specific adhesion events when DOPC:Chol bilayers were probed, while the Young's modulus channel did reveal local heterogeneities in the mechanical properties (Fig. S6). This also indicates that the derivatized tip does not induce the Chol-enriched domains. In addition, probing the interaction between θ toxin tip and DOPC:SM bilayers did not display any specific adhesion events (Fig. S2d-f), confirming the specificity of the θ toxin tip for Chol domains.

Conclusions

While Young's modulus has already been used as criterium to put in evidence lipid domains on cells[18], we showed here for the first time that specific mapping using AFM tips derivatized with toxin fragments targeting specific lipids appears as a novel complementary and/or alternative approach to evidence lateral lipid heterogeneities at high-resolution (~10 nm lateral resolution). We believe that this technique could open new avenues for the development of novel platforms to decipher lateral lipid organization from lipid model surfaces to living cells under native conditions.

Acknowledgements

The research of the authors is financially supported by the Fonds National de la Recherche Scientifique (F.R.S.-FNRS grant numbers: PDR T.0090.15 to D.A.), the Research Department of the Communauté française de Belgique (Concerted Research Action), the Université catholique de Louvain (Fonds Spéciaux de Recherche), the 'MOVE-IN Louvain' Incoming post-doc Fellowship programme and the Salus Sanguinis Foundation. D.A. is a Research Associate of the FNRS. We thank Drs. A. Miyawaki, M. Abe and T. Kobayashi (Riken Brain Science Institute, Saitama, Japan & University of Strasbourg, France) as well as H. Mizuno (KU Leuven, Belgium) for supplying the Dronpa-NT-Lysenin and Dronpa-theta-D4 plasmids.

Conflicts of interest

There are no conflicts to declare.

References

1. D. Lingwood and K. Simons, *Science*, 2010, **327**, 46-50.
2. K. Simons and M. J. Gerl, *Nat. Rev. Mol. Cell Biol.*, 2010, **11**, 688-699.
3. K. Bacia, D. Scherfeld, N. Kahya and P. Schwille, *Biophys. J.*, 2004, **87**, 1034-1043.
4. J. E. Shaw, R. F. Epand, R. M. Epand, Z. Li, R. Bittman and C. M. Yip, *Biophys. J.*, 2006, **90**, 2170-2178.
5. M. Carquin, L. D'Auria, H. Pollet, E. R. Bongarzone and D. Tyteca, *Progress in Lipid Research*, 2016, **62**, 1-24.
6. A. Makino, M. Abe, M. Murate, T. Inaba, N. Yilmaz, F. Hullin-Matsuda, T. Kishimoto, N. L. Schieber, T. Taguchi, H. Arai, G. Anderluh, R. G. Parton and T. Kobayashi, *The FASEB Journal*, 2015, **29**, 477-493.
7. F. Spira, N. S. Mueller, G. Beck, P. von Olshausen, J. Beig and R. Wedlich-Soldner, *Nat Cell Biol*, 2012, **14**, 890-890.
8. H. Kuge, K. Akahori, K.-i. Yagyu and K. Honke, *Journal of Biological Chemistry*, 2014, **289**, 26783-26793.
9. D. Fitzner, A. Schneider, A. Kippert, W. Möbius, K. I. Willig, S. W. Hell, G. Bunt, K. Gaus and M. Simons, *The EMBO Journal*, 2006, **25**, 5037-5048.
10. Y. Shimada, M. Maruya, S. Iwashita and Y. Ohno-Iwashita, *European Journal of Biochemistry*, 2002, **269**, 6195-6203.
11. M. Carquin, L. Conrard, H. Pollet, P. Van Der Smissen, A. Cominelli, M. Veiga-da-Cunha, P. J. Courtoy and D. Tyteca, *Cellular and Molecular Life Sciences*, 2015, **72**, 4633-4651.
12. H. Shogomori and T. Kobayashi, *Biochimica et Biophysica Acta (BBA) - General Subjects*, 2008, **1780**, 612-618.
13. R. Ishitsuka and T. Kobayashi, *Anatomical Science International*, 2004, **79**, 184.
14. M. Carquin, H. Pollet, M. Veiga-da-Cunha, A. Cominelli, P. Van Der Smissen, F. N'kuli, H. Emonard, P. Henriet, H. Mizuno, P. J. Courtoy and D. Tyteca, *Journal of Lipid Research*, 2014, **55**, 1331-1342.
15. A. A. Waheed, Y. Shimada, H. F. G. Heijnen, M. Nakamura, M. Inomata, M. Hayashi, S. Iwashita, J. W. Slot and Y. Ohno-Iwashita, *Proc. Natl. Acad. Sci. U. S. A.*, 2001, **98**, 4926-4931.
16. R. Ishitsuka, A. Yamaji-Hasegawa, A. Makino, Y. Hirabayashi and T. Kobayashi, *Biophys. J.*, 2004, **86**, 296-307.
17. D. Alsteens, H. E. Gaub, R. Newton, M. Pfreundschuh, C. Gerber and D. J. Müller, *Nat. Rev. Mat.*, 2017, **2**, 17008.
18. A. Dumitru, M. Poncin, L. Conrard, Y. Dufrene, D. Tyteca and D. Alsteens, *Nanoscale Horizons*, 2018, DOI: 10.1039/C7NH00187H.
19. Y. F. Dufrêne, D. Martinez-Martin, I. Medalsy, D. Alsteens and D. J. Muller, *Nat. Methods*, 2013, **10**, 847-854.
20. D. Alsteens, M. Pfreundschuh, C. Zhang, P. M. Spoerri, S. R. Coughlin, B. K. Kobilka and D. J. Müller, *Nat. Methods*, 2015, **12**, 845-851.
21. T. Bhatia, F. Cornelius and J. H. Ipsen, *Nature Protocols*, 2017, **12**, 1563.
22. C. S. Theile, M. D. Witte, A. E. M. Blom, L. Kundrat, H. L. Ploegh and C. P. Guimaraes, *Nature Protocols*, 2013, **8**, 1800.
23. H. Hertz, *Journal für die reine und angewandte Mathematik*, 1882, **92**, 156-171.
24. L. Redondo-Morata, M. I. Giannotti and F. Sanz, *Langmuir*, 2012, **28**, 12851-12860.
25. R. M. A. Sullan, J. K. Li, C. Hao, G. C. Walker and S. Zou, *Biophysical Journal*, 2010, **99**, 507-516.
26. T. S. Ursell, W. S. Klug and R. Phillips, *Proceedings of the National Academy of Sciences*, 2009, **106**, 13301-13306.

